Direct observation of the infinite percolation cluster in thin films: Evidence for a double percolation process

Pablo Jensen, Patrice Melinon, Michel Treilleux, Jian Xiong Hu, Jean Dumas, Alain Hoareau, and Bernard Cabaud

Département de Physique des Matériaux, Université Claude Bernard Lyon-1, 43 Bd. du 11 Novembre 1918, F-69622 Villeurbanne CEDEX, France

(Received 31 July 1992; revised manuscript received 2 November 1992)

Direct observation of the infinite percolation cluster at the percolation threshold is shown. We use crystallization propagation in an amorphous thin film. The morphological analysis of the infinite cluster shows good agreement with that predicted by percolation theory. The crystallization process can be described using an invasion percolation model in a fractal network. At the macroscopic scale, crystallization induces a double percolation.

I. INTRODUCTION

Percolation theory has become a powerful tool in the modeling of many natural systems where connectivity plays the leading role. A very active field is the modeling of thin-film growth (for a recent review, see Ref. 1). Experimentally, many groups have argued that the insulator-conductor transition observed during the growth of metallic thin films on insulator substrates could be understood in the framework of the percolation model.[2–5] So, optical[6] and magnetic[7] properties of thin films at thicknesses near the conduction threshold are extensively explained from percolation scaling laws. Yet, a major challenge is to know whether the morphology of the film at the conduction threshold is well described by the percolation idea.[8,9] Let us examine the case of antimony thin films prepared by molecular beam deposition. Owing to the high mobility of the incident particles (Sb_4 molecules), nucleation is governed by diffusion and occurs on preferential nucleation sites.[10] The supported particles have a roughly spherical shape and their diameter increases by engulfing the diffusing Sb_4 molecules. Dynamic and static coalescences and Ostwald ripening induce correlations in the bond distribution. This will affect typical properties of percolation such as the threshold coverage. We have found a threshold coverage of about 95%. Beghdadi[11] finds, on Au films, values ranging from 59 to 65 % depending on experimental conditions. Voss, Laibowitz, and Alessandrini[12] obtain thresholds around 74%. We recall that for *random* percolation, the threshold coverage is around 50%. Qualitatively the spread of threshold coverages can be explained by changes in the size distribution of the supported particles or/and variations in the distribution of nucleation sites on the substrate. The stronger the nucleation is, the more sensitive the threshold becomes to the substrate surface state. These preliminary results show that the interpretation of the growth of thin films from molecular beam deposition in terms of percolation theory faces some difficulties. Still, many researchers[5,11–13] have argued that, even for molecular beam deposition, the morphology of the film at the insulator-metallic transition is similar to that expected from percolation. To support this hypothesis, they have measured on their films several scaling laws, the fractal dimension of the infinite cluster (IC), and have found that these agree with those predicted by the percolation theory. Yet, there is a major experimental objection to those studies. We have noticed when performing the image analysis of our films that two unreconcilable requirements arise (see also Refs. 1, 5, and 14). The first is that a low microscope image magnification is needed to get a large collection of deposited particles to obtain good statistics when checking the scaling laws. The second is that a high-resolution image with high magnification is absolutely necessary to detect the connection between the particles. Other technical problems arise such as the digitization of the image, the correction of nonhomogeneous effects, and the thresholding method for binarization. These problems have, of course, been noticed and a few techniques which reduce their effects have been published.[15] Still, usually, low magnification micrographs are used and it is supposed that the connections are retained after binarization. We have found out that, at least in our films, this is not true. While the low magnification image does not show any evident connection, a high magnification image clearly shows the contrary (Fig. 1). To solve these problems, we have developed a physical method to get directly the infinite cluster without mathematical handling. This method uses the specific property of antimony thin films to crystallize through the connected particles. The basic idea is to crystallize *only* the IC, leaving the rest amorphous. Then, since crystallized particles are easily detected in transmission electron microscopy (TEM) micrographs, detection by high-resolution TEM (HRTEM) of the connection between two particles is superfluous. Indeed, even for a low magnification TEM image, only the particles connected to the IC will be detected, since only these (crystallized) particles show a high contrast with respect to the amorphous background. In the first part of this paper we show the results of the IC analysis.

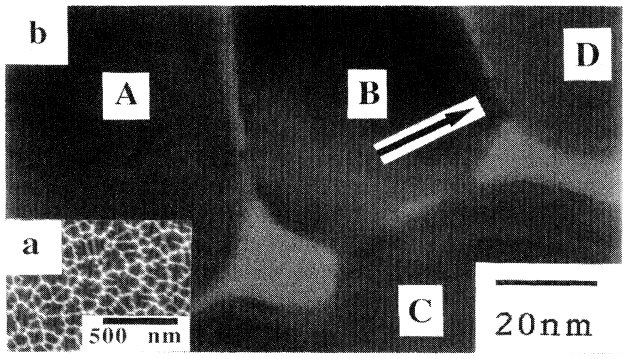

FIG. 1. TEM observation of antimony film at 17 nm thickness. (a) TEM observation at low magnification, the particles appear isolated. (b) HRTEM observation, at high magnification the bridges between the particles are clearly observed. Islands *A*, *B*, and *C* are crystallized (in bulk antimony lattice). The distances (not seen in this figure) between the planes {012} and {101} are, respectively, 0.311 and 0.354 nm. *D* is in the amorphous phase. The arrow indicates the direction of the crystallization hull.

In a second part a phenomenological model of the crystallization mechanism is given.

II. EXPERIMENTAL DETAILS

The antimony metal heated at about 580 °C is vaporized and deposited at room temperature on different substrates (residual pressure 10^{-4} Pa). For this residual pressure, bulk oxydation of the entire sample could be anticipated. We then perform AES (Auger electron spectroscopy) and XPS (x-ray photoelectron spectroscopy) studies using an UHV Nanoscan-100 (Cameca-Riber system) equipped with a MAC2 spectrometer. We studied the $3d_{3/2}$ and $3d_{5/2}$ transition rays of antimony. We observed a splitting of each of these rays into two, the shifts corresponding to the existence of Sb_2O_5. A profile depth showed no splitting in the bulk of the films. Then our antimony films present only partial surface oxydation. The absence of UHV conditions (10^{-4} Pa) does not allow a rigorous study of the nucleation mechanism. Indeed, in this range of vacuum values, the substrate characteristics (number of defects, impurities concentrations) cannot be determined. However, we have checked that for fixed experimental conditions (same substrate temperature, same deposition rate), our crystallization experiments were reproducible. The reason is the following. The number of nucleation sites is a function of preparation conditions, so the number of droplets and the fractional coverage corresponding to the incipient infinite cluster fluctuates. These fluctuations affect the absolute value of the thickness threshold (20% variation from sample to sample). The point is that the crystallization mechanism and the geometry of the IC are not determined by these parameters.

For transmission electron microscopy characterizations, the antimony was deposited on copper microscopy grids coated successively with 5-nm-thick *a-C* and 10-nm-thick SiO_2 films. In these conditions, we have checked that conductivity versus thickness characteristics are similar on Corning 7059 and on SiO_2 films. TEM observations were performed using a Philips EM 300 electron microscope and HRTEM observations were performed using a Jeol 200CX microscope. The analysis of the images was performed in an imaging hardware based on a hexagonal lattice. This lattice corresponds to the more packing structure of particles in the two-dimensional (2D) amorphous network.

The thickness is simultaneously controlled by a crystal quartz rate monitor. To measure the desorption rate on the substrate, the thickness of the deposit was checked by Rutherford backscattering spectrometry (RBS). To follow the growth of the film, electrical measurements are performed *in situ*. Antimony is deposited on Corning 7059 glass substrates with two predeposited chromium electrodes. The applied potential is 1 V and the minimum measurable conductance with our device is about 2×10^{-14} S. Then TEM micrographs give the morphology of the IC and electrical measurements give an estimate of the insulator-metal transition corresponding to the incipient IC.

III. GROWTH OF ANTIMONY FILMS: AN OVERVIEW

The growth of antimony thin films has already been extensively studied by several workers. It has been established that (see Refs. 10 and 16–22 and references therein) (a) the incident Sb_4 molecules nucleate on preferential sites, giving rise to islands whose diameters increase with matter deposition (three-dimensional layer growth);[10,18] (b) below a critical thickness almost all supported antimony particles are in the amorphous state, a few particles are crystallized;[20] (c) above the critical thickness, crystallization occurs,[10,19,20] the few crystallized particles are some embryos of the amorphous film crystallization;[20] (d) the critical thickness corresponds to

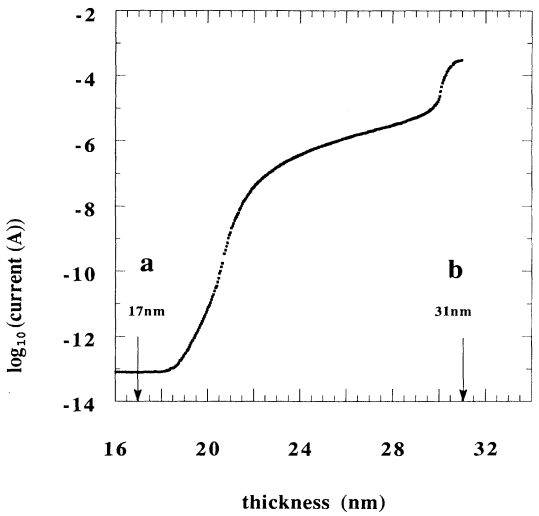

FIG. 2. Experimental current vs thickness curve obtained at room temperature. Deposition rate: 0.05 nm s^{-1}. The arrows show the particular thicknesses observed in TEM. The *a* arrow corresponds to Figs. 1 and 3. The *b* arrow corresponds to the crystallization of the continuous thin film.

the thickness at which the film becomes almost continuous;[21,22] (e) the crystallization rate increases with increasing film temperature. It also increases with increasing film thickness because the bridges connecting the islands become larger and larger. For films below the critical thickness, the crystallization rate is too slow to act and an energy (electron bombardment, for example) must be added. For thicker films, crystallization occurs rapidly at room temperature without additional energy.

IV. STUDY OF THE INFINITE CLUSTER

To be able to control the process, we have deposited a thin film, stopping the deposition slightly before the conduction threshold (arrow *a*, Fig. 2), when the bridge sections between the droplets are small and the crystallization rate is negligible at room temperature. We have a "stable" amorphous film, yet with a quasi-infinite cluster. Then we just have to choose a totally amorphous region, close to a crystallized embryo, and irradiate it with the microscope beam to increase locally the crystallization rate and see the crystallization spread among the islands connected to the (locally) "infinite" cluster. It should be observed that, upon contact, droplets do not coalesce to form large particles (after crystallization, the shape of each particle remains unchanged). So, the lattice geometry (created by all the particles) will be considered as invariable. Having obtained by this physical method the "infinite" cluster without any mathematical thresholding, we can now study it and compare its morphology with that predicted by percolation theory.

Figure 3 shows the IC. The values of the fractal dimensions of the whole IC and that of its hull (all the crystallized particles that are connected to the infinite cluster and are neighbors to amorphous particles) have been measured. The value of the fractal dimension of the IC is (Fig. 4) $D_f = 1.91 \pm 0.01$, while that of the *hull* is $D_h = 1.7 \pm 0.05$ in the large size range, while for small sizes we get a homogeneous distribution ($D = 1.1 \pm 0.1$). These measured fractal dimensionalities are in good

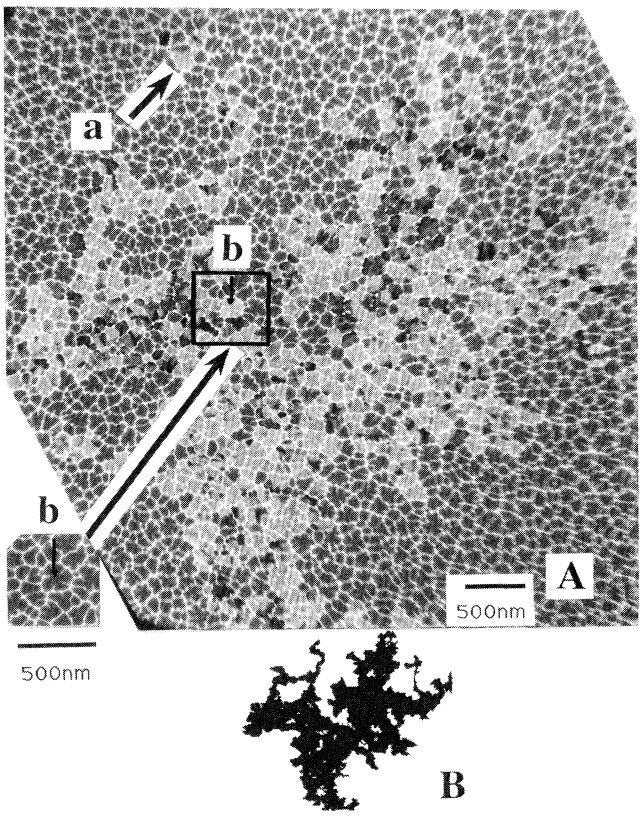

FIG. 3. (A) TEM observation of antimony film corresponding to arrow *a* (Fig. 2). Particles corresponding to a dark grey color are in the amorphous phase. Crystallized particles show a strong contrast (pale grey or dark). The diffraction patterns (not shown) corroborate these assumptions. The isolated particle (labeled *a*) is crystallized but not connected to the amorphous network. So, this particle is not a center of crystallization. The *b* windows show the initial and the final states (before and after crystallization) of a network part. Network geometry remains unchanged. (B) Binary image (256×256 bits) of the crystallized network.

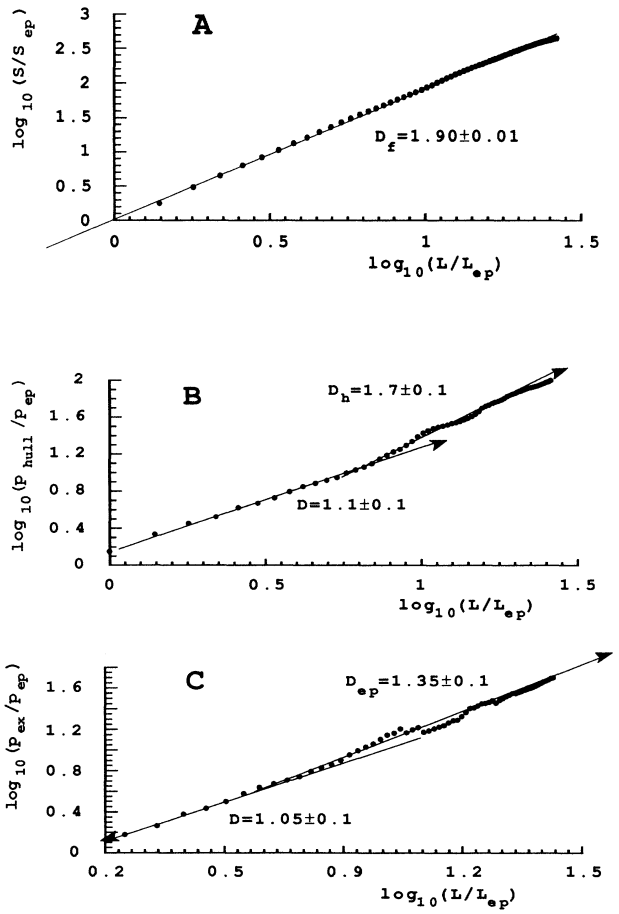

FIG. 4. Fractal dimensions. Each elementary particle can be compared to a hexagon of $S_{ep} = 19$ pixels surface. The corresponding length and perimeter are called, respectively, L_{ep} and p_{ep}. For a typical window of analysis the studied parameters are S, L, and p. (A) Fractal dimension of the IC. (B) Fractal dimension of the hull. p_{hull} is the perimeter of the hull. (C) Fractal dimension of the external perimeter. p_{ex} is the external perimeter.

agreement with those predicted by percolation theory: $D_f = \frac{91}{47}$ (Ref. 23) and $D_h = 1.75$.[24,25] Then we can conclude that percolation is a good model to describe the morphology of the IC of thin films near the conduction threshold.

V. CRYSTALLIZATION DYNAMICS

Crystallization allowed us to mark off the IC. We are now going to study crystallization in greater detail: first its dynamics at the microscopic scale and then its macroscopic effects, studied by electrical measurements.

A. Microscopic scale: Invasion percolation in a fractal network

Let us first study the crystallization dynamics. Figure 5 gives different crystallization steps at different times. The final image, Fig. 3, shows the stationary state beyond which no appreciable change is observed. The dynamics of crystallization are very close to that of invasion percolation (progression by bursts) as observed by Furuberg *et al.*[26] We propose a model of double percolation that, we claim, appropriately describes our system. For simplicity we shall describe our model in a square lattice but an extension to other types of lattices is straightforward. In a homogeneous lattice, we give to each bond a random number p $(0 < p < 1)$ just as in *bond* ordinary percolation. Then we arbitrarily choose a critical value p_c and change the p values for each bond to a value r according to the following rule: if $p < p_c$ then $r = p$ and if $p > p_c$, $r = 0$.

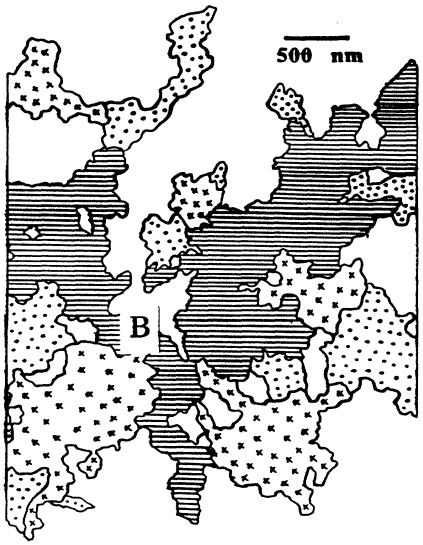

FIG. 5. Time evolution of the network: the dashed area is obtained after 10 minutes. The area corresponding to the sum of the dashed area and the (x) indexed area is obtained after 20 minutes. The area corresponding to the sum of the dashed area, the (x) indexed area, and the $(\cdot)$ indexed area, is obtained after 30 minutes. This time corresponds to the final state. The area labeled *B* corresponds to the area labeled b of Fig. 3.

Then a modified percolation invasion is performed, starting in an arbitrarily chosen bond. We recall that in conventional invasion percolation the growth of the cluster is performed by occupying the perimeter bond that has the highest (or the smallest) r value. Here we choose to invade, at each step, a given bond, but the probability to choose a given bond is now *proportional* to its r. Our model is then, in some sense, less deterministic than conventional invasion percolation. Still, we guess that the main features of the clusters generated by this model are the same as in the conventional one. It would be interesting if theoreticians could investigate this model further. Some comments are now necessary. First we see that, at infinite time, only the sites with $r \neq 0$ will be occupied. Then by choosing p_c equal to the ordinary percolation threshold, we see that only the IC will be invaded if the initial bond has been chosen within it. Clearly, to reproduce our experiments, r should be chosen as a function of the bridge section connecting the two islands ($r \propto S$, where S is the bridge section, for example).

We should now add an important remark: it could be argued that the values of the fractal dimensionalities attributed to the IC could correspond to those of the percolating cluster obtained by invasion percolation. What we have called the IC would just have been a cluster generated by the invasion percolation mechanism. In fact, fractal dimensionalities of this latter cluster are identical with those of ordinary percolation.[25] There is yet a conclusive argument in favor of ordinary percolation: the final fractional coverage. Indeed, the latter hypothesis would lead to the fact that all the sites would be invaded (crystallized) at a sufficient long time. In our experiment the final fractional coverage is close to 40%. This clearly invalidates the invasion percolation hypothesis and is in good agreement with ordinary percolation (in ordinary percolation, the infinite cluster shows a fractional coverage of about 45% at the threshold; for a square lattice, see Ref. 27.

B. Macroscopic scale: Double electrical percolation

Growth of antimony thin films has been extensively studied by the means of electrical measurements (see Ref. 17 and references therein). Electrical measurements are a sensitive method to study crystallization of the samples. It was then interesting to see what implications the preceding phenomena (as observed at the microscopic scale) could have in the electrical characteristics of the samples. Let us first go back to Fig. 2 to remind us of the main characteristics of the electrical behavior of antimony thin films as the thickness is increased.[17,28] Below 18.5 nm, the supported particles are well separated, allowing no detectable current to cross the sample. Then a first current jump occurs, indicating an insulator-conductor transition. This jump has been observed by many groups[1] working on evaporation of thin metallic films and is interpreted as the percolation of the metallic phase. Then, the first current jump of Fig. 2 can be attributed to the percolation of the amorphous phase [recall that the particles are essentially amorphous, point (b)].

This is confirmed by the absolute magnitude of the conductance around 21 nm, characteristic of amorphous antimony. At this stage, many amorphous islands begin to be connected with their neighbors. As explained previously, the crystalline structure propagates along the sample. Eventually, a continuous *crystalline* path crosses the sample, joining the two electrodes. Then it seems reasonable to interpret the second jump at 30 nm as the percolation of the crystalline phase among the amorphous one. This has been confirmed by electron microscopy observations.[17] We have shown elsewhere[28] a mean-field model that confirms qualitatively that the two jumps are effectively related to two transitions: isolating to amorphous first and amorphous to crystalline after.

VI. CONCLUSION

From this experiment we have shown that the infinite cluster corresponding to the formation of the first *continuum* path in the film is well described by correlated bond percolation, therefore percolation scaling laws must be adequate to explain phase transitions in thin films. Thanks to our physical method, we have avoided difficulties arising from the necessity of both low-high magnification images to analyze correctly the morphology of the films. Finally, we think that it would be useful to compare quantitatively crystallization propagation to ordinary invasion percolation, especially concerning the dynamics of the invasion.[27,29]

[1]P. Smilauer, Contemp. Phys. **32**, 89 (1991).

[2]M. Octavio, G. Gutierrez, and J. Aponte, Phys. Rev. B **36**, 2461 (1987).

[3]J. A. J. Lourens, S. Arajs, H. F. Helbig, El-Sayed A. Mehanna, and L. Cheriet, Phys. Rev. B **37**, 5423 (1988).

[4]L. Cheriet, H. H. Helbig, and S. Arajs, Phys. Rev. B **39**, 9828 (1989).

[5]P. Gadenne, A. Beghdadi, and J. Lafait, J. Microsc. Spectrosc. Electron. **12**, 477 (1987).

[6]Y. Yagil and G. Deutscher, Appl. Phys. Lett. **52**, 373 (1988).

[7]A. Gerber and G. Deutscher, Phys. Rev. Lett. **63**, 1184 (1989).

[8]This is surely the case for the low-energy cluster beam deposited film. There the diffusion coefficient of the incident particles (the clusters) is weak and growing the film is analogous to tiling the substrate with the incident clusters. Then, continuum site percolation is a good model to understand the insulator-metallic phase transition (Ref. 9).

[9]P. Melinon, P. Jensen, J. X. Hu, A. Hoareau, B. Cabaud, M. Treilleux, and D. Guillot, Phys. Rev. B **44**, 12 562 (1991).

[10]G. Fuchs, P. Melinon, F. Santos Aires, M. Treilleux, B. Cabaud, and A. Hoareau, Phys. Rev. B **44**, 3926 (1991).

[11]A. Beghdadi, Ph.D. thesis, Université Paris VI, 1986.

[12]R. Voss, R. Laibowitz, and E. Alessandrini, Phys. Rev. Lett. **49**, 1441 (1982).

[13]A. Kapitulnik and G. Deutscher, Phys. Rev. Lett. **49**, 1444 (1982).

[14]A. Kapitulnik and G. Deutscher, Thin Solid Films **113**, 79 (1984).

[15]A. Beghdadi, A. Constans, P. Gadenne, and J. Lafait, Rev. Phys. Appl. **21**, 73 (1986).

[16]J. Xiong Hu, Ph.D. thesis, Université Claude Bernard Lyon-1, 1993.

[17]A. Hoareau, J. Xiong Hu, P. Jensen, P. Melinon, M. Treilleux, and B. Cabaud, Thin Solid Films **209**, 161 (1992).

[18]F. Santos Aires, Ph.D. thesis, University of Lyon, France, 1990.

[19]M. Hashimoto and T. Nohara, Thin Solid Films (to be published).

[20]G. Fuchs, M. Treilleux, F. Santos Aires, P. Melinon, B. Cabaud, and A. Hoareau, Thin Solid Films **204**, 107 (1991).

[21]K. Maki, Jpn. J. Appl. Phys. **12**, 148 (1973).

[22]A. Barna, P. B. Barna, G. Raddnoczi, and I. Rechenberg, Acta Tech. Sci. Hung. **100**, 281 (1977).

[23]D. Stauffer, *Introduction to Percolation Theory* (Taylor and Francis, London, 1985).

[24]R. F. Voss, J. Phys. A **17**, L373 (1984).

[25]J. Feder, *Fractals* (Plenum, New York, 1988).

[26]L. Furuberg, J. Feder, A. Aharony, and T. Jfssang, Phys. Rev. Lett. **61**, 2117 (1988).

[27]A. Kapitulnik, A. Aharony, G. Deutscher, and D. Stauffer, J. Phys. A **16**, L269 (1983).

[28]P. Jensen, P. Melinon, A. Hoareau, J. X. Hu, M. Treilleux, and B. Cabaud, J. Phys. (Paris) **2**, 365 (1992).

[29]C. K. Peng, S. Prakash, H. J. Herrmann, and H. E. Stanley, Phys. Rev. A **42**, 4537 (1990).

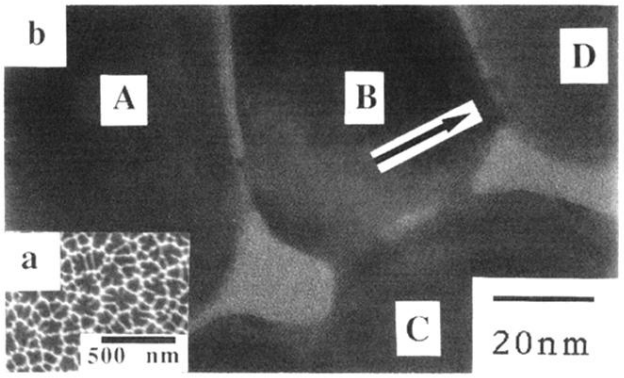

FIG. 1. TEM observation of antimony film at 17 nm thickness. (a) TEM observation at low magnification, the particles appear isolated. (b) HRTEM observation, at high magnification the bridges between the particles are clearly observed. Islands *A*, *B*, and *C* are crystallized (in bulk antimony lattice). The distances (not seen in this figure) between the planes {012} and {101} are, respectively, 0.311 and 0.354 nm. *D* is in the amorphous phase. The arrow indicates the direction of the crystallization hull.

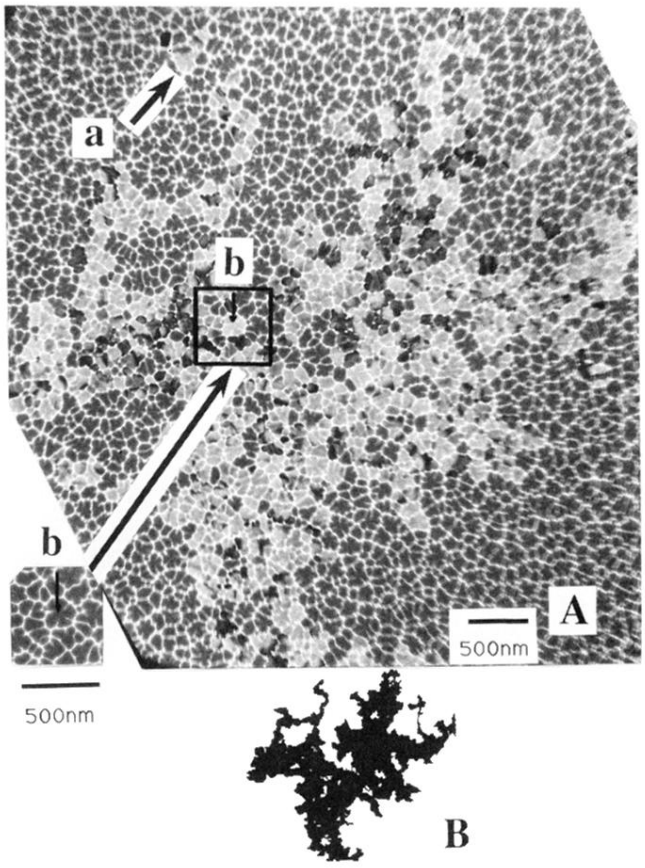

FIG. 3. (A) TEM observation of antimony film corresponding to arrow *a* (Fig. 2). Particles corresponding to a dark grey color are in the amorphous phase. Crystallized particles show a strong contrast (pale grey or dark). The diffraction patterns (not shown) corroborate these assumptions. The isolated particle (labeled *a*) is crystallized but not connected to the amorphous network. So, this particle is not a center of crystallization. The *b* windows show the initial and the final states (before and after crystallization) of a network part. Network geometry remains unchanged. (B) Binary image (256×256 bits) of the crystallized network.